

RESEARCH

Open Access



Targeting glutamine synthetase with AS1411-modified exosome-liposome hybrid nanoparticles for inhibition of choroidal neovascularization

Miaomiao Zhang^{1†}, Xinyue Lu^{1†}, Lifu Luo², Jinqiu Dou¹, Jingbo Zhang¹, Ge Li¹, Li Zhao¹ and Fengying Sun^{1*}

Abstract

Choroidal neovascularization (CNV) is a leading cause of visual impairment in wet age-related macular degeneration (wAMD). Recent investigations have validated the potential of reducing glutamine synthetase (GS) to inhibit neovascularization formation, offering prospects for treating various neovascularization-related diseases. In this study, we devised a CRISPR/Cas9 delivery system employing the nucleic acid aptamer AS1411 as a targeting moiety and exosome-liposome hybrid nanoparticles as carriers (CAELN). Exploiting the binding affinity between AS1411 and nucleolin on endothelial cell surfaces, the delivery system was engineered to specifically target the glutamine synthetase gene (GLUL), thereby attenuating GS levels and continuously suppressing CNV. CAELN exhibited spherical and uniform dispersion. In vitro cellular investigations demonstrated gene editing efficiencies of CAELN ranging from 42.05 to 55.02% and its capacity to inhibit neovascularization in HUVEC cells. Moreover, in vivo pharmacodynamic studies conducted in CNV rabbits revealed efficacy of CAELN in restoring the thickness of intra- and extranuclear tissues. The findings suggest that GS is a novel target for the inhibition of pathological CNV, while the development of AS1411-modified exosome-liposome hybrid nanoparticles represents a novel delivery method for the treatment of neovascular-related diseases.

Introduction

Age-related macular degeneration (AMD) is an ophthalmic condition characterized by irreversible vision loss or deterioration resulting from degenerative lesions affecting the retinal pigment epithelium and retina. AMD ranks as the world's third most prevalent cause of blindness after cataracts and glaucoma [1, 2]. The underlying

mechanism of AMD involves mainly long-term inflammation, lipofuscin, and increasing number of vitreous warts. Dry AMD typically advances gradually, but untreated it may progress to wet AMD (wAMD), which has a blindness rate of more than 80% [3]. wAMD is pathologically characterized by the invasion and penetration of choroidal neovascularization (CNV) into the Bruch's membrane, which leads to vascular leakage, hemorrhage, fibrosis, and eventual vision impairment. Currently, the clinical treatment for wAMD primarily involves the use of vascular endothelial growth factor (VEGF) inhibitors, mainly including vitreous cavity injection of ranibizumab [4, 5], VEGF-Trap (abciximab injection) [6], and bevacizumab injection [7]. However,

[†]Miaomiao Zhang and Xinyue Lu contributed equally to this work.

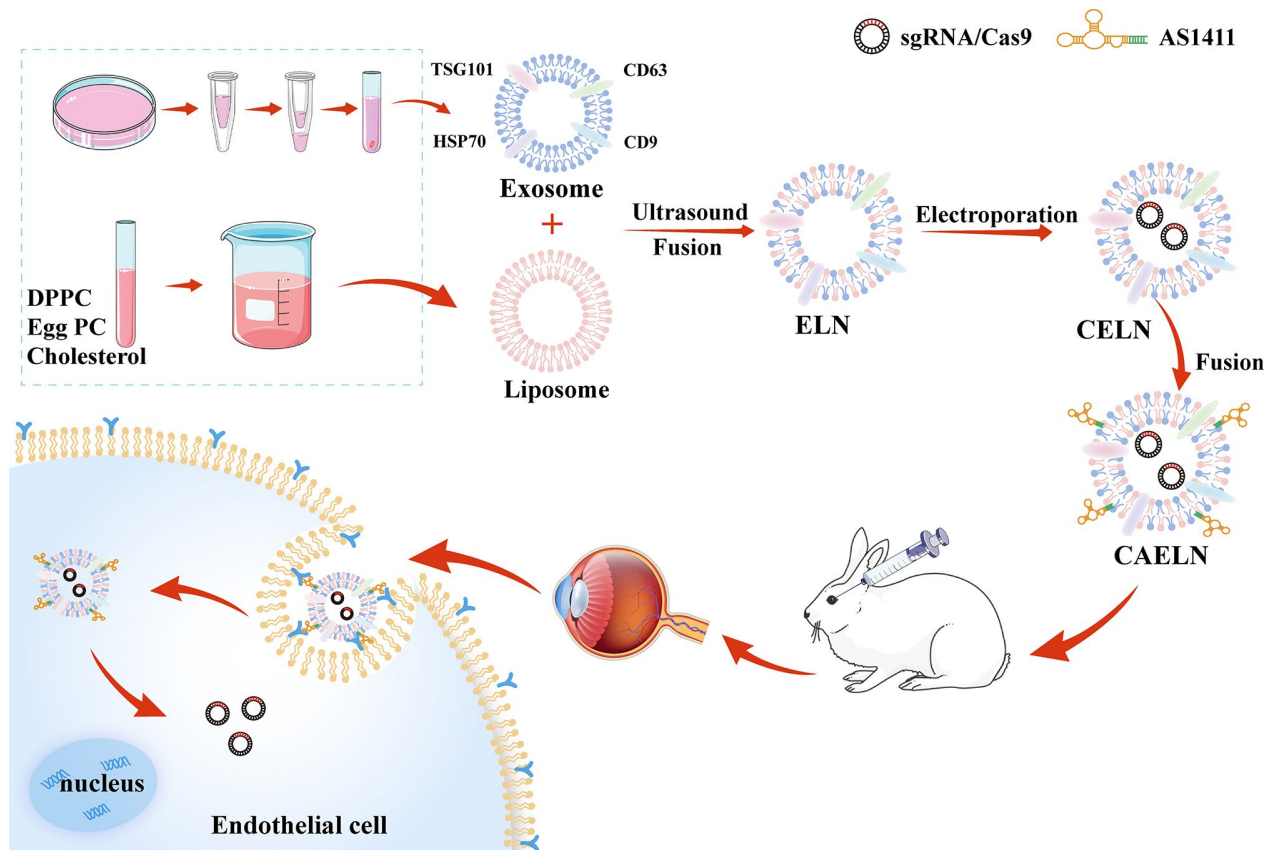
*Correspondence:
Fengying Sun
sunfengying@jlu.edu.cn

Full list of author information is available at the end of the article



© The Author(s) 2024. **Open Access** This article is licensed under a Creative Commons Attribution-NonCommercial-NoDerivatives 4.0 International License, which permits any non-commercial use, sharing, distribution and reproduction in any medium or format, as long as you give appropriate credit to the original author(s) and the source, provide a link to the Creative Commons licence, and indicate if you modified the licensed material. You do not have permission under this licence to share adapted material derived from this article or parts of it. The images or other third party material in this article are included in the article's Creative Commons licence, unless indicated otherwise in a credit line to the material. If material is not included in the article's Creative Commons licence and your intended use is not permitted by statutory regulation or exceeds the permitted use, you will need to obtain permission directly from the copyright holder. To view a copy of this licence, visit <http://creativecommons.org/licenses/by-nc-nd/4.0/>.

Graphical abstract



Keywords CRISPR/Cas9, Choroidal neovascularization, Exosome, Liposome, Glutamine synthetase, Age-related macular degeneration, Vascular endothelial growth factor, Nucleic acid aptamer

some patients may develop resistance to anti-VEGF drug therapy [8]. Patients often need repeat vitreous injections, which not only poses a financial burden, but also leads to poor patient compliance and risk of complications [9]. Therefore, it is necessary to search for new targets to inhibit pathological CNV in order to improve the inadequacy of existing therapies and enhance the quality of life of patients.

Glutamine synthetase (GS), the product of the *GLUL* gene, functions as an ATP-dependent synthetase primarily responsible for catalyzing the production of glutamine from ammonia and glutamate [10]. Endothelial cells (ECs), located in the luminal layer of blood vessels, express GS and their metabolism controls angiogenesis. It has been reported that making vascular endothelial cells glutamine deficient or inhibiting glutamine affects vascular endothelial cell migration and reduces ocular neovascularization [11, 12]. Inhibition of GS results in reduced levels of the protein RHO J which maintains the acylation and membrane localization and migration

activities of RHO J. Therefore, affecting cell migration by knocking down the *GLUL* gene inhibits pathological angiogenesis [13–15], and this approach could also be used to treat ocular neovascularization-related diseases.

Compared to current conventional therapies for wAMD, this approach not only enhances the effectiveness of long-term drug therapy but also has the potential to reduce the need for repeated treatments by directly targeting the underlying cause of the disease. Additionally, it exhibits minimal side effects on normal tissues throughout the treatment process [16]. In contrast to other gene knockout systems, clusters of regularly interspaced short palindromic repeat sequences (CRISPR)/CRISPR-associated protein (Cas) system presents distinct advantages characterized by superior efficiency, cost-effectiveness, and reliable knockout efficacy [17, 18]. CRISPR/Cas system, originating from the adaptive immune mechanisms of bacteria and archaea, facilitates precise genome editing by inducing DNA double-stranded breaks (DSBs) at specific genetic sites. This

type-II CRISPR/Cas system consists of the DNA nucleic acid endonuclease Cas9, CRISPR RNAs (crRNAs), and trans-activating crRNAs (tracrRNAs). It is widely applied across various fields, encompassing human, animal, plant, and microbial genome manipulation [19, 20]. Currently, a major challenge facing the clinical translation of CRISPR/Cas9 systems is the absence of effective and safe delivery methods. Traditionally, CRISPR/Cas9 systems are delivered in vivo using viral vectors, including lentiviral, adenoviral, and adeno-associated virus (AAV) vectors [21]. Nonetheless, the potential cytotoxicity, immunogenicity, and sustained expression of viral vectors continue to impede clinical application. Recently, non-viral delivery methods have emerged, including lipid nanoparticles and Cas9 protein/gRNA ribonucleoprotein complexes, although they are constrained by limited stability, safety, and delivery efficiency [22, 23].

Exosomes, ranging from 30 to 150 nm in diameter, are lipid membrane-bound nanovesicles secreted by cells. They can be extracted from diverse extracellular fluids, such as blood, urine, and cellular supernatants. Exosomes play a pivotal role in facilitating intercellular communication, which holds significance in both clinical disease diagnosis and treatment [24–28]. In recent years, researchers have sought to address the low efficiency of exosomes in encapsulating large nucleic acid segments by developing exosomes and liposomes hybrid nanoparticles (ELN) by mixing liposomes and exosomes [29]. In contrast to conventional exosomes, ELN exhibit enhanced capability to encapsulate larger plasmids, such as CRISPR/Cas9 expression vectors. This feature makes them highly promising for applications in in vivo gene editing. Choroidal capillaries are permeable vessels comprising a single layer of endothelial cells and pericytes within their walls. Choroidal capillaries are permeable vessels and CNVs form highly permeable vessels. Considering these aspects, hybrid exosomes, approximately 200 nm in size, can effectively traverse the vessel wall to access endothelial cells [4, 30].

AS1411 is a guanosine-rich nucleic acid aptamer that forms a G-quadruplex structure, providing resistance against nuclease degradation. Single-stranded DNA containing CG sequences can be constructed into metal-polyDNA nanoparticles to achieve the appropriate biological function, as well as to immobilize enzymes and protect enzymes [31, 32]. Single-stranded DNA enriched with CG sequences can also be used as a tool for targeted delivery. AS1411 exhibits a selective binding affinity for nucleolin protein (NCL), which enters the cell to disrupt normal cell replication and proliferation [33–35]. Previous studies have indicated that AS1411 also holds promise as a therapeutic agent for CNV [36, 37]. NCL is not only abundantly expressed on the surface of tumor cells, but is also significantly expressed on

the membrane surface of neovascular cells. AS1411, as a highly structured aptamer, was used to activate the preparation of a DNA nanoreactor that can specifically recognize and tightly bind to NCL on the surface of tumor cells by AS1411 to achieve in vivo tumor imaging results [38]. The selective recognition of AS1411 can also be exploited for binding to NCL [39]. In this study, we constructed AS1411-modified nanocarriers targeting ECs based on ELN and delivered the CRISPR/Cas9 system (CAELN) that can knock down the GLUL gene, expecting to silence the relevant genes at the molecular level for the treatment of wAMD. Meanwhile, the safety and neovascularisation inhibition of the delivery system were evaluated at cellular and animal levels, providing a new idea for nanomedicine-mediated specific gene editing for AMD treatment.

Materials and methods

Reagents

For Liposomes prepared in certain proportions, DPPC, EggPC and cholesterol were used. Endothelial cell culture medium (ECM) and DMEM culture medium (containing 1% L-glutamine), fetal bovine serum (FBS), penicillin, and streptomycin were purchased from Pricella (China). AS1411 nucleic acid aptamer was purchased from Shanghai Biotechnology. Anti-CD63 and anti-TSG101 antibodies were purchased from Bioss. Plasmid design and construction involved using an online CRISPR design tool to create CRISPR/sgRNAs targeting the GLUL gene, obtained from Hanbio Biotechnology Co., Ltd. (Shanghai, China). The two sgRNA sequences are 5'-ACGGAA GGGGTCCCGAAACA-3' and 5'-GCACACCTGTAAA CGGATAA-3'.

Cell lines and animals

The HEK293T, A-RPE and HUVEC cells were purchased from Pricella (China) and cultured in medium with 10% FBS and 1% antibiotics in DMEM and ECM at 37 °C with 5% CO₂. All animal testing conducted in this study received ethical approval from Jilin University and was carried out in strict compliance with relevant laws and regulations. Experimental Animal Technology Co., Ltd. (License number: SYXK (JI) 2020-0004) supplied New Zealand white rabbits, specifically males aged 6 ~ 8 weeks and weighing between 2.0 ~ 2.5 kg.

Preparation of ELN

HUVEC cells were grown in DMEM containing 10% FBS, 1% L-glutamine, 100 U/mL penicillin, and 100 mg/mL streptomycin. Once the confluence reached 70–80%, HUVEC cells were transitioned to fresh medium without FBS, replacing DMEM for 48 h. The cell supernatant was centrifuged at 2,000 g for 15 min at 4 °C in order to remove any remaining cells and debris. A subsequent

centrifugation at 10,000 g for 15 min removed smaller debris. Exosome Precipitation Solution-Cell Media (EPS-C) was added to the cell supernatant, and the cells were subjected to overnight incubation at 4 °C. The following day, centrifugation was performed on the cells at a speed of 10,000 g for 30 min at 4 °C, with removal of the liquid portion above the sedimented cells and retention of the exosome precipitate. Finally, the exosomes were resuspended in ERS-C for immediate use or cryopreserved at -80 °C.

Liposomes were prepared using the ethanol injection method. Egg yolk lecithin, DPPC, and cholesterol were weighed in a specific ratio. Then, 1 mL of anhydrous ethanol was added, and the organic phase was injected into 10 mL of water or PBS preheated to 50 °C. The solution was agitated for a duration of 45 min at a speed of 500 rpm using a magnetic stirring device. The liposomes were then prepared under vacuo conditions and stored at 4 °C.

The liposomes and exosomes prepared in advance were combined at a mass ratio of 5:1. The mixture was subjected to ultrasonication in an ice bath using 80 W power with a pulse duration of 2 s on/off for a total of 2 min. Subsequently, the exosome-liposome hybrid nanoparticles were obtained by allowing the liposomes to incubate in a 37 °C water bath for 1 h after the initial mixing. The occurrence of membrane fusion between the two components and the optimal fusion ratio were verified using the FRET assay.

FRET assay: Liposomes were labelled with DiI and DiD dyes and fused with exosomes to prepare ELN by the above method. The fluorescence intensity of the two dyes was detected by a fluorescence spectrophotometer, and compared with the liposomes alone, the increase in the intensity of the DiI fluorescence and decrease in the intensity of the DiD fluorescence indicated the success of fusion of the exosomes with the liposomes.

Plasmid design and construction

The synthesized vector was transfected into HEK293T cells, and after a designated transfection period, the transfection impact was examined using a fluorescence inverted microscope. The knockdown efficacy of the two sequences was confirmed through Western blotting and RT-PCR. Then, the sgRNA sequences exhibiting superior knockdown effects were selected for further experiments. The subsequent sgRNA is denoted as sgRNA2.

Preparation of sgRNA/Cas9@ELN (CELN)

ELN and sgRNA/Cas9 plasmid were combined in a 5:1 ratio (100 µL) and transferred to a 0.1 cm electroporation cuvette. Electroporation was performed using an exponential pulse of 125 µF capacitance at 180 V. The samples were then incubated at 4 °C for 1 h to promote membrane

recovery. The product sgRNA/Cas9@ELN after electroporation and membrane recovery is called CELN.

AS1411 modified sgRNA/Cas9@ELN (CAELN)

To prepare a 2 mg/mL solution of cholesterol, 6 mg of cholesterol was dissolved in sterile water to achieve a total volume of 3 mL. Additionally, 10 OD of nucleic acid aptamer was added to 1 mL of sterile water to formulate a solution. Next, 1 mL of the cholesterol solution was used, followed by the addition of equal moles of EDC and NHS. The cholesterol was activated by stirring for 2 h at room temperature. Following this, nucleic acid aptamers were introduced and stirred at room temperature, resulting in AS1411-modified cholesterol obtained after overnight dialysis. Finally, AS1411-modified sgRNA/Cas9-loaded hybrid exosomes were prepared by integrating AS1411 on CELN membranes through the affinity of cholesterol for phospholipid bilayers, creating what is referred to as CAELN.

To further confirm the successful modification of CELN by the AS1411 aptamer, a conjugate was created using DiI-labeled CELN and 3'6-FAM-labeled AS1411. The conjugation between AS1411 and CELN was assessed using fluorescence co-localization imaging under a fluorescence microscope.

Characterization of CAELN

A specialized analyzer was used to evaluate the size of nanoparticles and their zeta potential, while the morphology of exosomes and liposomes was examined using transmission electron microscopy (TEM) (JEM-2100 F, Nippon Electron Co., Ltd.). Briefly, exosomes were added to a copper grid, negatively stained with 2% uranium dioxide acetate for exosomes visualization, washed twice with deionized water, dried overnight, and subsequently imaged using the microscope.

Western blotting

To confirm the existence of exosome membrane proteins on both exosomes and CAELN, total proteins were extracted from the mentioned cells, exosomes, or CAELN using RIPA lysate with added PMSF and sodium protovanadate for 30 min at 4 °C. Following protein quantification using the BCA kit, the proteins were adjusted to match the cell lysate concentration and mixed with 5×Sodium Dodecyl Sulfate-Polyacrylamide Gel Electrophoresis (SDS-PAGE) Protein Loading Buffer at a 1:4 dilution. The mixture was then boiled at 95 °C for 10 min. Samples containing 30 µg of total protein each were loaded onto SDS-PAGE gel for electrophoresis. Proteins were then transferred from the gel to a polyvinylidene difluoride (PVDF) membrane. Subsequently, the membrane was blocked with 5% skimmed milk powder (w/v) for 2 h at room temperature, followed by

overnight incubation at 4 °C with primary antibodies (CD63, TSG101, and HSP70) diluted in appropriate concentrations. The membrane underwent incubation with enzyme-labeled secondary antibodies at room temperature for 1 h. Following a final wash, protein bands were visualized and detected using an ECL kit and a chemiluminescent imaging system, respectively.

Quantitative RT-PCR (qRT-PCR)

Total RNA was extracted from distinct groups of cells 48 h post-transfection. The extracted RNA underwent reverse transcription using a two-step method, generating cDNA. The cDNA was then amplified using a PCR instrument. Subsequently, the cells were combined with 2×RealStar Green Fast Mixture with ROX II reagent, distributed into eight consecutive rows corresponding to different groups, with six replicate wells in each group. The mixture was transferred to the ABI7500 instrument for RT-PCR experiments, and the results were analyzed.

Fluorescence inversion microscopy to detect transfection effect

After reaching 80–90% cell fusion in HEK293T cells, 6-well plates were prepared. Cells were seeded onto plates at a density of 2.5×10^6 cells per well, and cultured until they reached 80% confluence before transfection. The transfection of CELN and CAELN was performed for 6–8 h. After discarding the old medium, fresh medium was added for further incubation for 48 h. Lipofiter 3.0 (Lipo) was used as a positive control for transfection. The effectiveness of transfection was then observed under a fluorescence-inverted microscope.

Cell immunofluorescence

Cells with 90% confluence were spread and transfected. The supernatant was removed, and cells underwent three washes with PBS. Fixation was carried out by adding 180 µL of 4% paraformaldehyde, shaking on a shaker for 20 min. Following fixation, cells underwent three PBS washes, and 500 µL of membrane-disrupting solution was applied for 20 min to aid permeabilization. Subsequently, cells underwent three PBS washes followed by the addition of a 2% BSA solution to each well. The plate was then placed on a shaker and allowed to incubate for a duration of 30 min. After removing BSA, cells were washed three times with PBS. A pre-prepared primary antibody was added, followed by the addition of a secondary antibody, and incubated at room temperature for 1 h at 4 °C overnight. After the allotted time, cells were washed three times with PBS. The process was repeated by adding the pre-configured primary antibody of the corresponding concentration and incubating overnight at 4 °C. Following that, cells were washed three times with PBS, and the secondary antibody was introduced, incubating at room

temperature for 1 h. Subsequently, after another three PBS washes, DAPI was applied to stain the cell nuclei for 5 min. Following another round of washing, the slides were mounted, protected from light, and the results were observed under the fluorescence microscope.

T7E1 cleavage assay

The transfected HUVEC cells were harvested, and total DNA was extracted using a DNA extraction kit. The concentration of DNA was then measured using a NanoDrop 2000 spectrophotometer. Two PCR primers were designed and employed to amplify the extracted DNA employing a high-fidelity polymerase. The amplification process involved denaturation at high temperature, annealed, and extension for 35 cycles. The resulting products underwent electrophoresis on a 1.2% agarose gel to confirm the presence of target bands at expected positions. After verification, T7E1 digestion was performed. The reaction system was prepared by adding reagents according to the instructions of Novozymes digestion kits. Following PCR, the digestion reagent was directly added to the mixture, which was then incubated at 37 °C for 37 min. Subsequently, to evaluate the digestion efficiency and confirm gene knockdown, 1.2% agarose gel electrophoresis was conducted again to assess the reaction termination.

In vitro cellular uptake

HUVEC cells were seeded onto a 12-well plate with coverslips and allowed to adhere overnight. Subsequently, the cells were treated with plasmids encapsulated with Cy5 fluorescent markers using different vectors. Following treatment, the samples underwent three washes with PBS. Subsequently, cells were immersed in a 4% paraformaldehyde solution, followed by DAPI staining of the nuclei for 5 min. Following staining, the samples were carefully transferred onto slides, inverted, sealed with a cover slip, and allowed to dry naturally. The uptake efficiency was observed under a confocal microscope with a light microscope to assess and visualize the cellular internalization of the labeled plasmids.

The outer membranes of ELN and AELN were labelled and stained with the lipophilic dye DiD. HUVEC cells, ARPE-19 cells, and HEK293T cells were seeded onto 6-well plates. When the cells reached 80% confluence, the original medium was replaced with medium containing DiD@ELN or DiD@AELN, and the cells were incubated for 4 h. To investigate concentration-dependent uptake characteristics, HUVEC cells containing different concentrations of DiD@AELN were added to HUVEC cells at 80% confluence. Additionally, cells incorporated with DiD@AELN were incubated for varying durations to assess time-dependent uptake of nanoparticles by the cells. After 4 h, cells were digested, and the targeting of

AS1411 in nanoparticles to different cells was assessed by flow cytometry at 644 nm. The concentration-dependent uptake characteristics of HUVEC cells for DiD@AELN were also evaluated. The experiment included incubating cells with DiD@AELN for different durations to observe the time-dependent uptake of nanoparticles by the cells.

Scratch wound migration assay

HUVEC cells, post-digestion, were plated in 6-well dishes at a density of around 5×10^5 cells per well. After reaching full confluence, a monolayer scratch was created using a 200 μL lancelet tip. The scratched monolayer was then washed three times with PBS to eliminate floating cells. Subsequently, serum-free medium containing the drug was added to the experimental group, while the control group received serum-free medium without the drug. The scratches were photographed and recorded using a 10 \times inverted microscope at 0 h. After 24 h of incubation, the migration area was measured using ImageJ software. The migration area of the control group was considered as 100%, and the migration area of the drug-treated group was expressed relative to this control. The inhibition rate of the drug on cell migration was calculated based on the comparison of migration areas between the drug-treated and control groups after 24 h of incubation.

Transwell invasion experiment

In the experiments, all materials were pre-cooled at 4 $^\circ\text{C}$ overnight. Transwell chambers were inserted into 24-well plates, and matrix gel was diluted according to a specific ratio and added to the upper chamber. The mixture was then allowed to solidify into a membrane at 37 $^\circ\text{C}$ for over 1 h. HUVEC cells (4×10^4) were added into the upper chamber, mixed with basal medium containing sgRNA/Cas9 plasmid, CELN, and CAELN. In the lower chamber, 500 μL of medium containing growth factors (VEGF₁₆₅) was added, allowing HUVEC cells to infiltrate. After 24 h, non-invaded cells on the upper chamber surface were removed, while the cells on the lower surface were fixed with paraformaldehyde and stained with crystal violet. Subsequently, after air-drying, the cells were photographed and observed under a 10 \times microscope. The number of invaded cells was quantified using ImageJ software, with the control group serving as the reference point set at 100%.

Tube formation assay

A 96-well plate was precooled overnight at 4 $^\circ\text{C}$. Then, 50 μL of diluted matrix gel was dispensed into each well, and the plates were incubated in a 37 $^\circ\text{C}$ incubator for over 30 min to allow for solidification of the matrix gel. HUVEC cells were then seeded at a density of 20,000 cells per well. A mixture of 100 μL of cell dilution and 100 μL of drug-containing medium was added to the wells

with matrix gel, and the cells were incubated for 4~6 h. Tubule formation was observed under an inverted microscope, and images were captured for documentation. The total branch length and branch number were assessed using ImageJ software to evaluate the effectiveness of drug in inhibiting tube formation in HUVEC cells, with the control group set as 100%.

CNV rabbit model experimental design

New Zealand white rabbits were used to establish a CNV rabbit model by laser photocoagulation. First, an argon green laser with the slit lamp and anterior lens wavelength adjusted to 532 nm, power of 0.75 W, and exposure time of 0.1 s was focused on the retina, avoiding large blood vessels. Then, 20 consecutive spots were irradiated in a dense area around the optic disc, approximately 2 to 3 optic disc diameters away from the disc edge, with each spot separated by 300 μm , and with each laser spot having a diameter of 50 μm . Successful coagulation was judged based on the generation of bubbles, which occurred after coagulation, demonstrating that Bruce's membrane had been broken by the laser. CNV rabbit model for macular degeneration was established in the right eyes of rabbits, while the left eyes served as the control. The rabbits in the Control group were not modeled. Fluorescein angiography (FFA) was used to determine if CNV rabbit model was successful. Then, the rabbits with successful modeling were randomly divided into 4 groups, which were CNV, sgRNA/Cas9, CELN, and CAELN. After 7 d, 50 μL of saline was injected into the vitreous of right rabbit eyes in the Control and CNV groups, while the other groups received vitreous injections of the same volume of drugs. After drug administration, levofloxacin ophthalmic ointment was applied topically twice daily for 14 days.

In vivo anti-angiogenic assessment

After 4 weeks of drug administration, FFA was conducted on the fundus of the right eyes in the Control, CNV, sgRNA/Cas9, CELN, and CAELN groups. After administering anaesthesia to the rabbits, serial photographs were initiated immediately upon intravenous injection of 2 mL of 2% fluorescein sodium at the ear margin for FFA examination. The FFA photographs were recorded using a high-performance digital imaging system (Kowa, Japan). The extent of neovascularisation in the right eyes of rabbits was examined and compared among the different groups.

Intraocular pressure (IOP) and weight assessment

IOP and body weight of rabbits were measured every week, both before and after the experiment. A handheld tonometer was placed perpendicular to the eye's center at a distance ranging from 2 to 10 mm and the angle of

90°. In order to avoid the experimental error, the measurement of each rabbit's eye in the different groups was repeated for 6 times, and according to the average value of IOP before the administration of the drug was used as the control, and the changes in the value of the IOP in each group were observed after the treatment.

Histopathological examination

After 4 weeks of vitreous administration, the rabbits were anesthetized and euthanized. Serial sections of the RPE-choroidal complex were prepared from the embedded eyeball specimens. These sections were made parallel to the sagittal axis of the optic nerve. Afterward, the sections were subjected to Hematoxylin-Eosin (HE) staining, fixed, and dried for observation.

Immunohistochemistry analysis

Following fixation of the right eyes of rabbits in each group, sections of the optic nerve sagittal axis-parallel RPE-choroidal complex were prepared. These sections underwent immunostaining to detect the GS protein. Positive staining, indicated by 3, 3'-diaminobenzidine brown coloration, was captured through microscopic observation. The optical density values of areas with positive staining in the choroid were analyzed and calculated using ImageJ software.

GS and inflammatory factors in RPE-choroidal complex

The eyes of rabbits from each group were carefully dissected to collect RPE-choroidal complex. Total protein was extracted by adding a specific amount of lysate containing protease and phosphatase inhibitors at 4 °C. The samples were mechanically pulverized using a ball mill, followed by centrifugation to collect the supernatant. The GS protein content was quantified using a rabbit GS ELISA kit. While rabbit-specific ELISA kits for IL-6, TNF- α , and IL1- β were used to determine the levels of the corresponding inflammatory factors.

Statistics

Student's *t*-tests were utilized to assess the significance between treated samples and controls, assuming a one-tailed distribution and equal variance for two samples. For data that did not follow a normal distribution, significance was determined using the one-tailed Mann-Whitney test in GraphPad Prism 6. For datasets involving multiple treatment groups, one-way ANOVA analysis was conducted using GraphPad Prism 6. A significance threshold of $P < 0.05$ was considered statistically significant.

Results

Synthesis and characterization of CAELN

In this study, liposomes were prepared using the ethanol injection method. Simultaneously, exosomes were extracted from HUVEC cell supernatants and subjected to membrane fusion (Fig. 1A). The characteristics of the prepared liposomes, exosomes, CELN and CAELN were examined by Malvern particle size analyzer. The particle size of these nanoparticles was about 140 nm, PDI was less than 0.3, and potentials were about -15 mV (Fig. 1B). Subsequently, transmission electron microscopy (TEM) was performed on the nanoparticles. Both liposomes and CAELN were observed to be uniformly dispersed and spherical, with liposomes displaying a typical bowl-top shape (Fig. 1C). In Fig. 1D, the successful synthesis of ELN was verified through FRET experiments. Western blotting experiments of the nanoparticles confirmed the presence of membrane proteins on the exosome surface, demonstrating the retention of exosome bioactivity during the synthesis process (Fig. 1E, Fig. S1).

During the encapsulation of sgRNA/Cas9 plasmid, we conducted screening of the addition ratio, analyzing the results through agarose electrophoresis. The encapsulated plasmid exhibited truncation in the up-sampling wells. Ultimately, we identified the optimal ratio of the nanoparticles and plasmid as 5:1 (Fig. 1F). For the modification of AS1411 on the CELN surface, we used a fluorescence spectrophotometer to detect the standard curvature of AS1411. The AS1411 linkage efficiency was calculated to be 39.7% by the resulting regression equation (Fig. 1G). Fluorescence co-localization imaging under a fluorescence microscope of DiI-labeled CELN and 3'-FAM-labeled AS1411 demonstrated the successful conjugation. The DiI-labeled CELN exhibited red fluorescence, while the 3'-FAM-labeled AS1411 displayed green fluorescence. Upon merging, the two fluorophores form an orange color (Fig. S2).

In vitro uptake ability of CAELN

By different concentrations of CAELN in HUVEC, 293T and A-RPE cells toxicity assay, it was found that the survival rate of all three types of cells was greater than 85%, indicating that our synthesized CAELN has a better safety profile in the range of 0.1–250 $\mu\text{g}/\text{mL}$ (Fig. S3). To assess the cellular uptake of nanoparticles, uptake experiments were conducted using HUVEC cells. The findings presented in Fig. 2A demonstrate that the uptake efficiency of the free plasmid was lower compared to the CELN group, suggesting a homing effect of the exosomes on HUVEC cells. The optimal uptake efficiency was observed after modification with AS1411, indicating that AS1411 enhances the targeting to HUVEC cells, facilitating the delivery of the plasmid to the nucleus for gene editing. Quantitative screening of HEK293T,

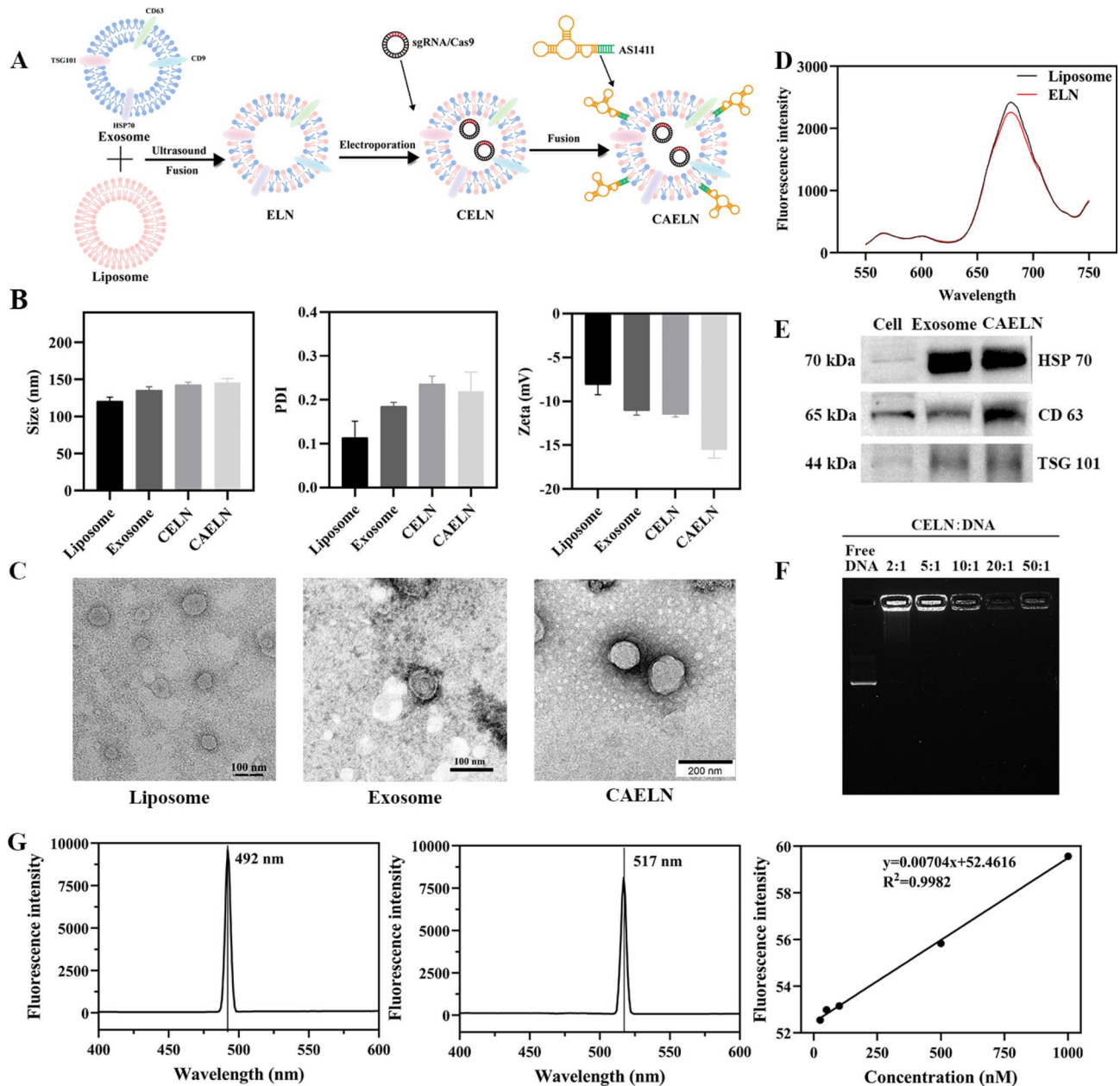


Fig. 1 Synthesis and characterization of CAELN. **(A)** The process of synthesizing exosome-liposome hybrid nanoparticles using ultrasound, demonstrating the hybridization and fusion of the membranes of exosomes and liposomes. **(B)** Particle size, PDI and Zeta potential of liposomes, exosomes, CELN, and CAELN, along with their TEM images **(C)**. **(D)** Images of DiD and Dil staining of liposomes and exosomes after FRET experiments, measured in a fluorescence spectrophotometer. **(E)** Western blotting images. **(F)** Agarose electropherograms after the addition of sgRNA/Cas9 plasmid at different ratios, with encapsulated sgRNA/Cas9 retained in the upwelled wells. **(G)** Excitation and emission wavelengths of AS1411 measured in a fluorescence spectrophotometer, along with the standard curve

A-RPE, and HUVEC cells by flow cytometry further confirmed the optimal uptake of the targeting group CAELN in HUVEC cells (Fig. 2B, E). HUVEC cells were subsequently exposed to varying concentrations of CAELN to observe the concentration dependence of uptake (Fig. 2C, F), revealing higher fluorescence intensity with increasing concentration. Similarly, time-dependent screening (Fig. 2D, G) demonstrated that the uptake reached

its maximum at 24 h. The enhanced targeting ability of AS1411 was shown to improve delivery efficiency and enhance gene editing.

In vitro transfection efficiency and gene editing ability of CAELN

To assess the in vitro transfection efficiency, HEK293T cells were transfected using Lipo as a transfection reagent

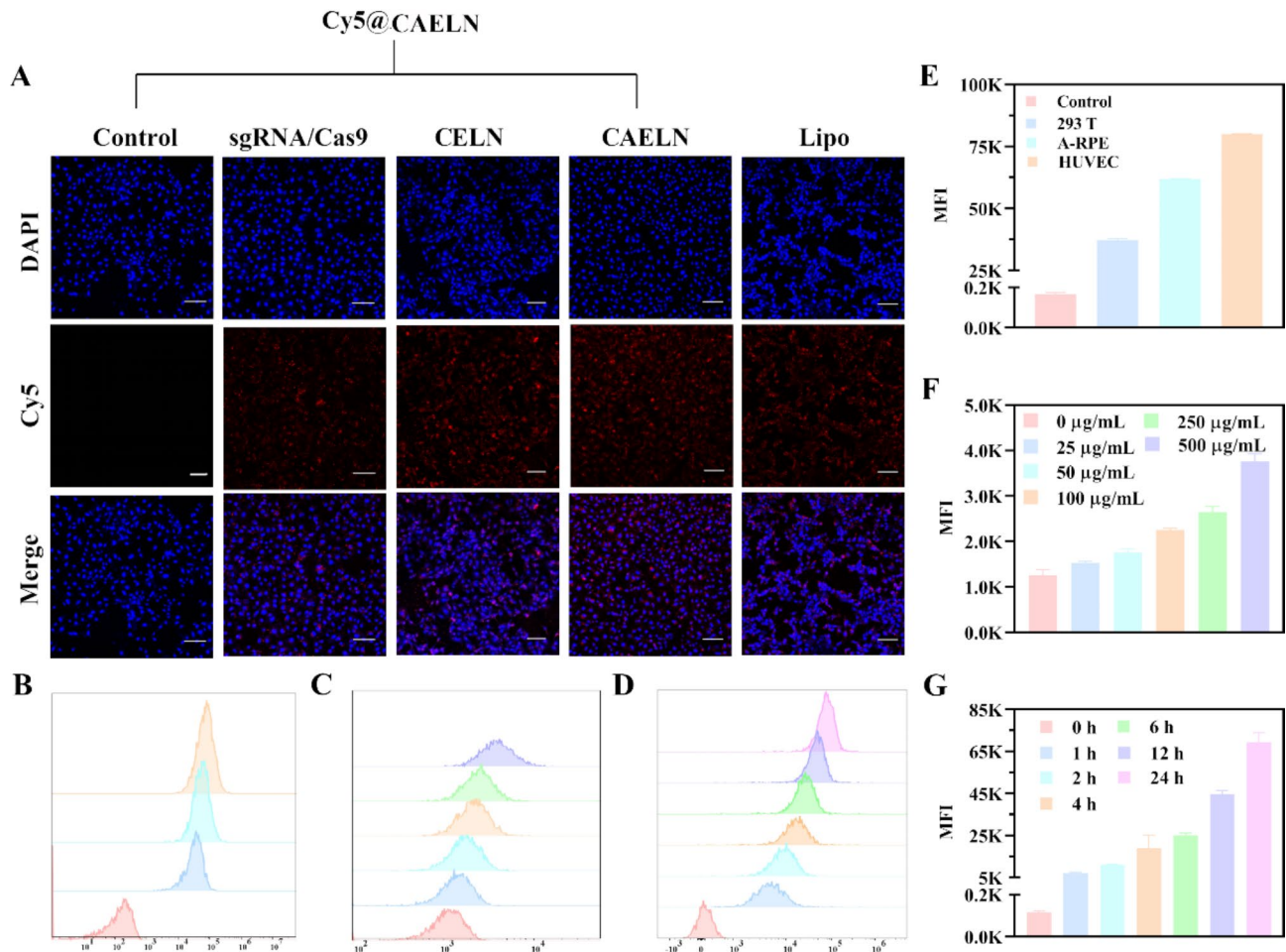


Fig. 2 Cellular uptake based on Cy5@AELN. **(A)** Fluorescence images (scale bar = 50 μ m) illustrating the uptake by HUVEC cells treated with different preparations. **(B, E)** Flow cytometry quantification of plasmid, Cy5@ELN, and Cy5@AELN uptake ($n=3$) by HEK293T, A-RPE, and HUVEC cells. **(C, F)** Uptake of different concentrations of AELN by HUVEC cells ($n=3$). **(D, G)** Uptake dependence on time ($n=3$)

encapsulated with the two sequences. Following transfection, fluorescence intensity was observed with a fluorescence inverted microscope, revealing that sgRNA2 exhibited a more effective sgRNA1 (Fig. 3A). Consistent results were obtained at the gene level through RT-PCR, and Western blotting analysis further confirmed that sgRNA2 demonstrated superior excision effect (Fig. 3B). CAELN was synthesized using the previously described method, and its transfection efficiency was examined in both HEK293T and HUVEC cells. The findings indicated that the transfection efficiency of CAELN exceeded that of the free plasmid and CELN, reaching levels comparable to those observed in the positive control group and Lipo group (Fig. 3C). The whole film is shown in Fig. S4. The introduction of AS1411-targeted ligands was validated to enhance transfection efficiency in both cell types.

The results were verified in both cell types evaluated the protein level by Western blotting experiments, where the narrower bands suggested a more effective knockdown

effect. Notably, the CAELN group showed the smallest band, consistent (Fig. 3D). RT-PCR experiments further simultaneously conducted the mRNA levels. The outcomes indicated a notable reduction in GLUL mRNA levels in sgRNA/Cas9, CELN, and CAELN groups compared to the control group, in line with the Western blotting findings (Fig. 3E). The GS ELISA kit also showed the same results as Western blotting (Fig. 3F). Meanwhile, in the immunofluorescence experiments, the CAELN group obtained significantly lower fluorescence intensity than the other groups, consistent with the above results (Fig. 3G). Additionally, the T7E1 digestion experiment verified the gene sequence after PCR amplification of the knockdown DNA fragment, demonstrating a high knockdown efficiency of 42.05% in the targeted group (Fig. 3H). In summary, these findings collectively demonstrate the successful knockdown of the GLUL gene using CRISPR/Cas9 system, with a significant and efficient effect.

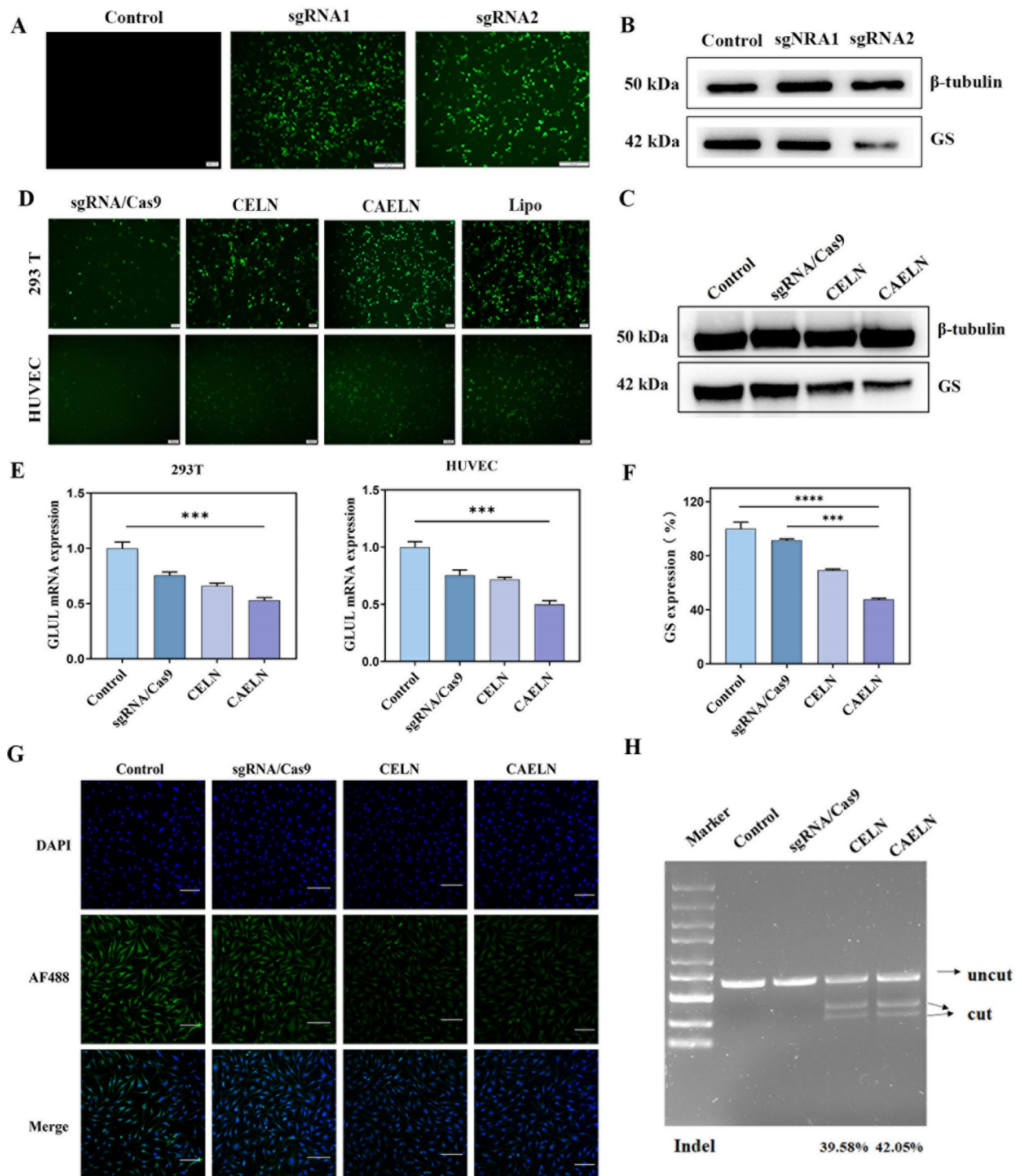


Fig. 3 In vitro transfection efficiency of CAELN. **(A)** Transfection effects observed by a fluorescence inverted microscope. **(B)** In vitro transfection of HEK293T and HUVEC cells with sgRNA/Cas9, CELN, CAELN, and Lipo. **(C)** Western blotting analyzed the gene editing effects ($n=6$). RT-PCR experiments **(E)** and GS ELISA kit **(F)** analyzed the gene editing effects of Control, sgRNA/Cas9, CELN and CAELN groups. **(G)** Immunofluorescence analysis of gene editing effects. **(H)** T7E1 digestion experiment. Significant differences were determined using one-way ANOVA. *** $P < 0.001$ and **** $P < 0.0001$

Inhibition of neovascularization capacity at the cellular level

As mentioned above, our synthesized CAELN demonstrated a significant gene knockdown ability in vitro, leading to the effective reduction of GS expression at both the protein and mRNA levels, successfully knocking down the GS gene in cells. Considering the positive correlation between GS presence and ocular neovascularization, we extended our assessment to cellular neovascularization in vitro. The knockdown of GLUL in HUVEC cells was found to decrease GTPase activity and activate other Rho GTPases, inducing actin stress and hindering endothelial cell migration [40]. The role and significance of GS in vascular sprouting were also highlighted, suggesting an inhibition of endothelial cell migration affecting neovascularization [41]. In the scratch assay, where monolayers

of HUVEC cells were scratched, the CAELN group effectively inhibited scratch healing compared to the control group after 12 h of incubation (Fig. 4A, B). Comparable outcomes were observed in the invasion assay (Fig. 4C, D). In the tube formation assay, there was a notable disparity in the ability of the targeted CAELN group to inhibit tube formation compared to the other groups (Fig. 4E, F). This indicates that CAELN can effectively target HUVEC cells and had a good ability to inhibit neovascularization in vitro.

In vivo animal modeling and editing effects of CAELN

As illustrated in Fig. 5A, New Zealand white rabbits, anesthetized and positioned near the optic axis of the right eye, were exposed to laser irradiation following previously defined conditions. After allowing a one-week

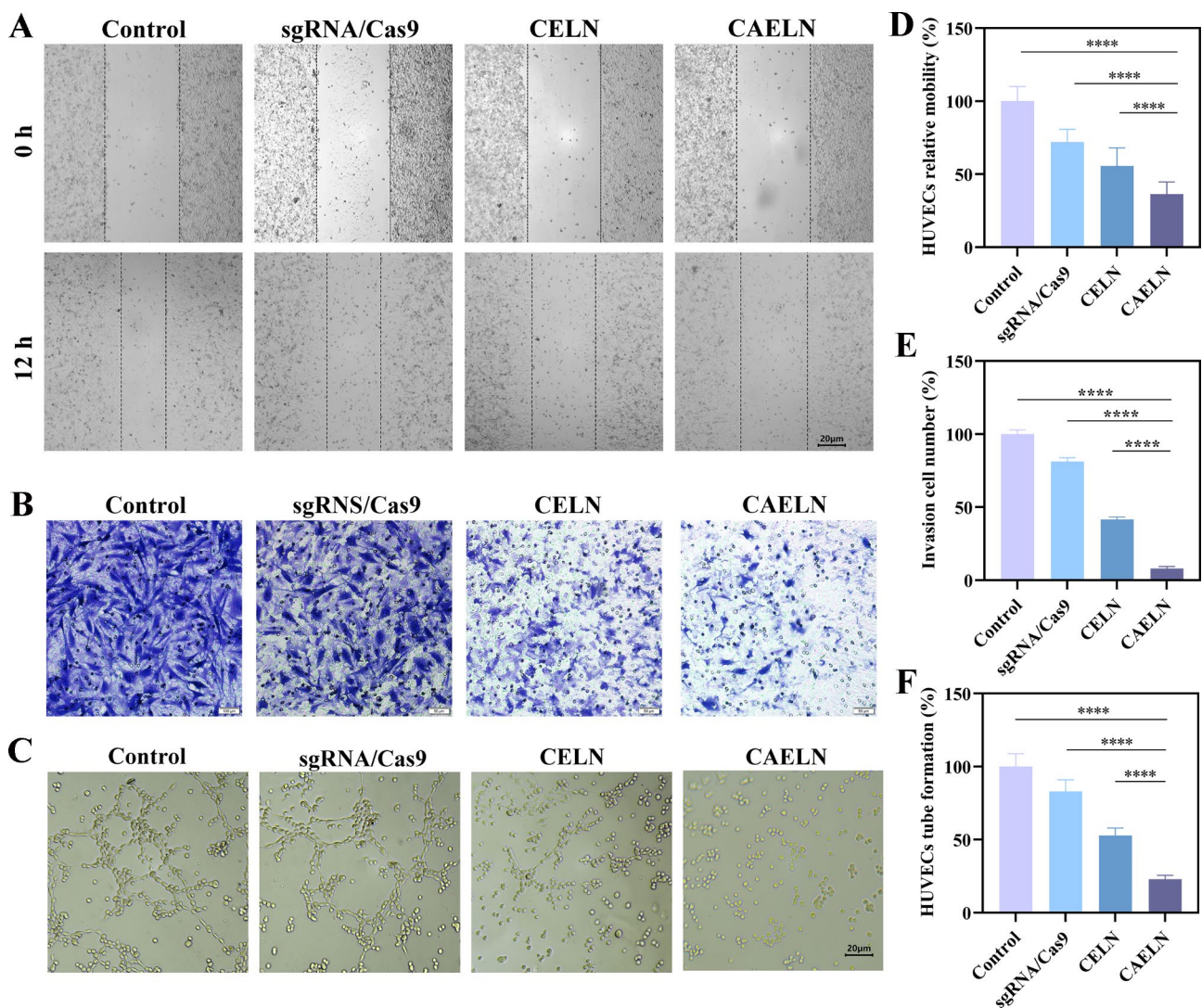


Fig. 4 The capacity of CAELN to inhibit cellular neovascularization. Scratch experiment (A) and quantification (D) ($n=3$). Transwell experiment (B) and quantification (E) ($n=3$). Tube formation experiments (C) and quantification (F) ($n=3$). Significant differences were determined using one-way ANOVA. **** $P < 0.0001$

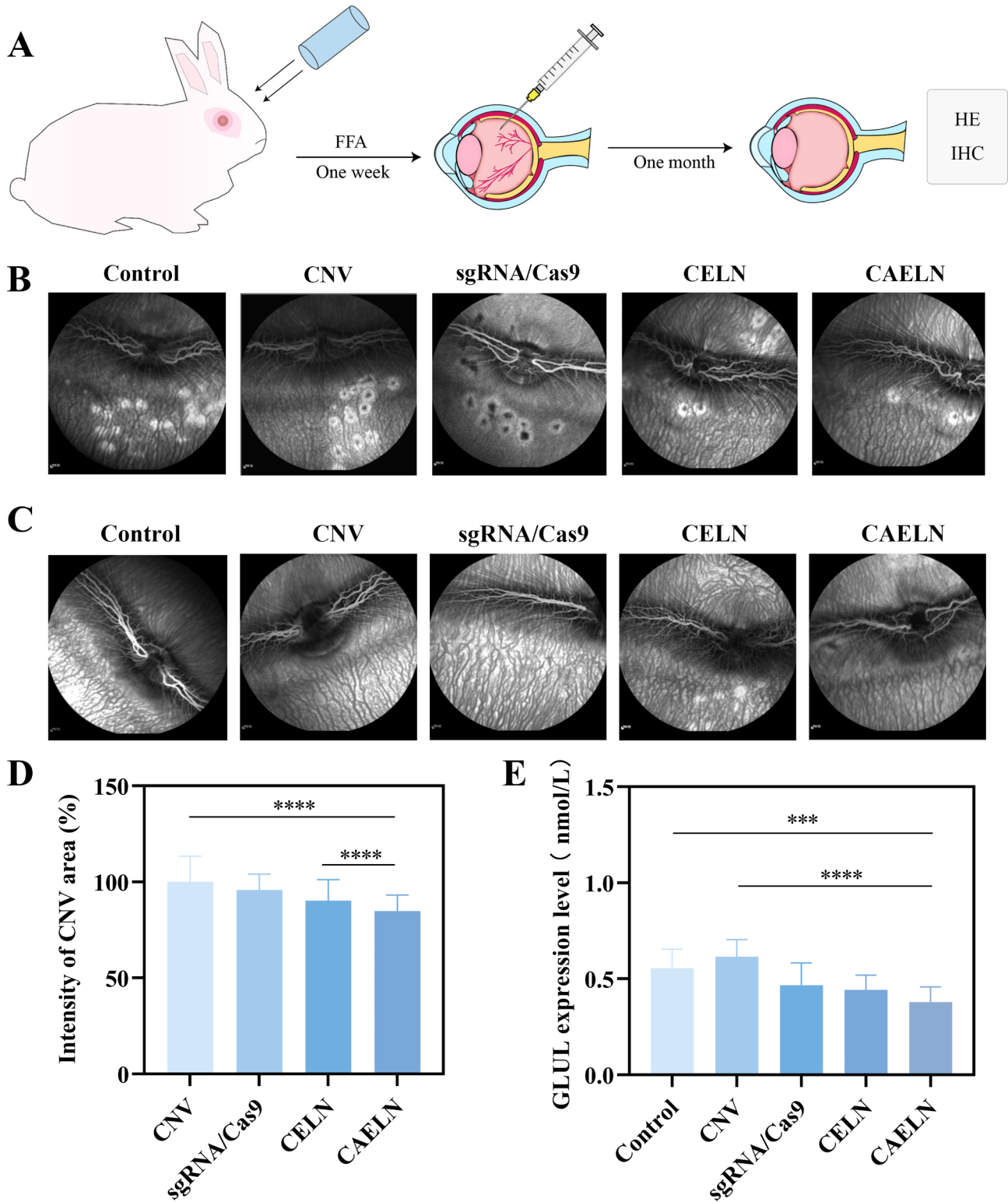


Fig. 5 (A) depicts the fabrication and treatment process of the CNV rabbit model. (B) and (C) present FFA images of the right eye of the rabbit before and after treatment, respectively. (D) provides quantitative analysis of neovascularization in each group of eyes in (C) ($n=3$). (E) is the ELISA determination of GS protein content in the RPE-choroid complex of the right eye. Significant differences were assessed using one-way ANOVA. *** $p < 0.001$ and **** $p < 0.0001$

period for the fundus to develop, FFA was conducted to assess neovascularization. Varying degrees of neovascular growth were observed in all rabbit groups (Fig. 5B). Subsequently, following successful modelling confirmation, the rabbits were treated with vitreous injections for one month. A month later, fundus FFA observations (Fig. 5C) and quantitative analysis of ocular neovascularization were conducted again (Fig. 5D). The neovascular growth in the CNV group served as a reference (100%) to evaluate the treatment effects in different groups. Both CELN and CAELN groups exhibited significant inhibition of neovascular growth, with CAELN demonstrating a more significant effect compared to CELN treatment (Fig. 5D). The results demonstrated a notable decrease in GS expression content in the CELN delivery group compared to the free plasmid group, indicating capacity of CELN for substantial plasmid delivery to the eye. Furthermore, the knockdown achieved by CAELN in the targeting group was optimized (Fig. 5E).

Safety evaluation

After euthanasia of rabbits in each group, the right eyes were dissected, fixed, and subsequently paraffin-embedded. Pathological sections and immunohistochemical analyses targeting GS proteins were conducted separately. The results revealed that the choroid in the normal rabbit group remained largely intact, showing no cellular atrophy in this layer. Conversely, the CNV group exhibited severe choroidal damage with an increased presence of inflammatory cells (Fig. 6A). Immunohistochemical assessments further indicated that the CAELN group demonstrated superior gene-editing effects, effectively reducing GS protein synthesis (Fig. 6B). Grey value analysis of GS protein content demonstrated a significant reduction in the CAELN group compared to the CELN group, emphasizing the targeting efficacy (Fig. 6E). As shown in Fig. S5, GS protein expression in the retina-choroid tissue of rabbit eyes, the CAELN group presented lower expression.

In the safety assessment of CAELN, it was found that the treatment we used did not induce notable alterations in the IOP and body weight of the rabbits (Fig. 6C, D). The intraocular pressure of the rabbits remained within a stable range. Moreover, the assessment of inflammatory factors in the RPE-choroid complex demonstrated that the treatment did not lead to a significant increase in inflammatory factors within the eyes of the rabbits (Fig. 6E, G and H).

Discussion

CNV presents a formidable challenge in ophthalmology, particularly in the context of wAMD, where it serves as a primary driver of irreversible vision loss [42]. In recent years, numerous studies have explored various

approaches to prevent CNV, including anti-angiogenic therapies targeting VEGF [43]. While these therapies have shown efficacy, they often require frequent injections and may have limited long-term benefits [44]. Thus, there is a pressing need for alternative strategies capable of providing sustained therapeutic effects with improved safety profiles.

Our study represents a significant advancement in this regard, as we introduce a novel approach using CAELN for targeted gene therapy against CNV. AS1411, an aptamer with high affinity for nucleolin overexpressed on endothelial cell surfaces, serves as an ideal ligand for targeted drug delivery [45]. By conjugating AS1411 to ELN, our aim was to achieve precise delivery of CRISPR/Cas9 components to target cells, thereby modulating neovascularization pathways. In our *in vitro* experiments, we demonstrated the superior transfection efficiency and gene knockdown efficacy of CAELN compared to conventional liposomes and free plasmid DNA. These findings align with previous studies highlighting the advantages of exosome-based delivery systems in achieving efficient gene delivery and therapeutic efficacy [46–48]. Importantly, we observed a significant reduction in GS expression, a key regulator of neovascularization, at both the protein and mRNA levels following treatment with CAELN. These findings underscore the potential of GS as a novel therapeutic target for CNV and highlight the efficacy of CRISPR/Cas9-mediated gene editing in modulating neovascularization pathways. Furthermore, *in vivo* studies using rabbit model of CNV provided further validation of the therapeutic efficacy of CAELN in inhibiting neovascular growth. Histopathological analyses revealed a significant reduction in GS expression and attenuation of CNV-associated pathological changes in the CAELN-treated group. Moreover, CAELN demonstrated superior gene-editing effects and targeted specificity, emphasizing its potential as a promising therapeutic intervention for neovascular-related diseases.

Comparing the findings with previous research underscores the innovative potential of CAELN in the landscape of ocular gene therapy. While prior studies have explored various gene therapy approaches for CNV, such as anti-VEGF therapies or gene editing strategies targeting other angiogenic factors, our approach offers distinct advantages in terms of targeted delivery, efficacy, and safety profile. Moreover, the ability of CAELN to achieve sustained therapeutic effects without the need for frequent injections represents a significant improvement over existing therapies. Looking ahead, there are several avenues for future research and development in this field. Optimization of CAELN formulation and delivery parameters will be crucial to enhance therapeutic efficacy and minimize potential side effects. Additionally, further preclinical studies are needed to evaluate the long-term

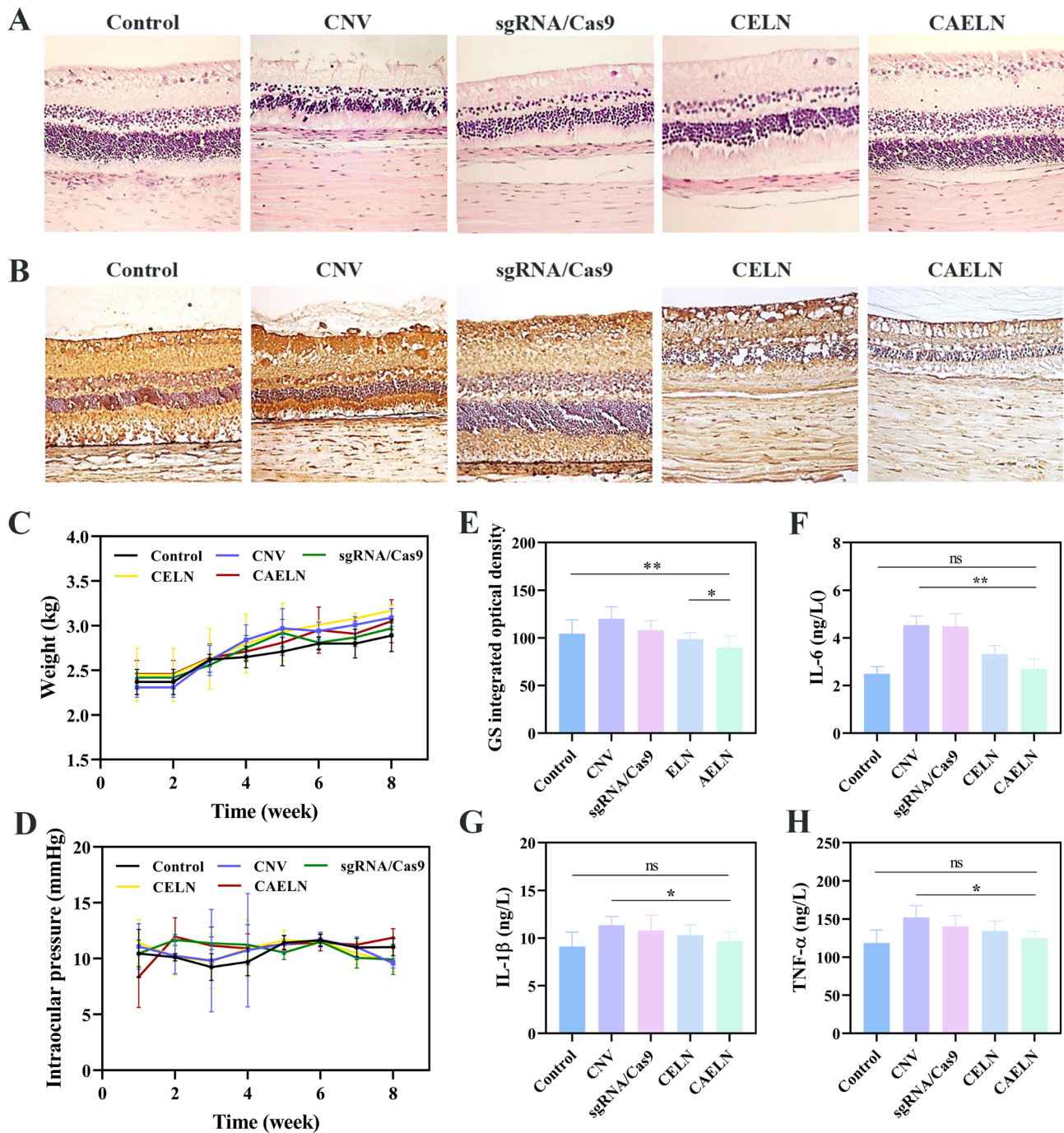


Fig. 6 (A, B) Immunohistochemical images of HE staining and GS of serial sections of the RPE-choroidal complex parallel to the sagittal axis of the optic nerve in the right eye, respectively (all images were obtained by photographing under a 200 \times microscope). (C, D) depict measurements of body weight and intraocular pressure during a specific period before and after the experiment ($n=3$). (E) represents the analyzed value of the optical density of GS in (B). (F, G and H) display ELISA measurements of the content of inflammatory factors in the RPE-choroid complex ($n=3$). Significant differences were determined using one-way ANOVA. * $P < 0.05$ and ** $P < 0.01$

safety and efficacy of CAELN in larger animal models and to assess its potential for clinical translation. Moreover, while our study focused on CNV in the context of wAMD, the therapeutic potential of CAELN may extend to other neovascular-related diseases, such as diabetic

retinopathy and retinopathy of prematurity [49]. In future studies, we will explore the applicability of CAELN in these disease contexts and elucidate its mechanisms of action. Therefore, our study represents a significant step forward in the development of targeted gene therapy

for CNV. By constructing AS1411-modified exosome-liposome hybrid nanoparticles, we have demonstrated the potential to achieve precise and efficient inhibition of neovascularization pathways, offering new hope for patients with CNV and related eye diseases. With further research and development, CAELN may emerge as a valuable therapeutic tool for the treatment of neovascular-related eye diseases.

Conclusion

We have developed a novel membrane hybrid vector by ultrasonic fusion, combining the modifiability of liposomes with the excellent biocompatibility and homing effect of exosomes. This unique vector facilitates targeted delivery to specific sites, enhancing therapeutic efficacy. Following AS1411 modification, CAELN nanoparticles exhibited improved targeting efficiency, with higher specificity for HUVEC cells than compared to HEK293T and A-RPE cells. CAELN demonstrated favorable particle size, and its remarkable ability to inhibit cell migration, invasion and angiogenesis *in vitro* was validated. The designed sgRNA showed efficient transfection effects in cells, and gene editing ability were confirmed through RT-PCR and Western blotting. *In vivo* studies using a rabbit model of CNV demonstrated a significant reduction in intraocular neovascularization with CAELN treatment, while avoiding a strong inflammatory response. The enhanced targeting properties of CAELN hold promise for future improvements, potentially allowing vascular injection to achieve effective inhibition of chorioidal neovascularization. Additionally, the gene editing system presents a potential for more sustained treatment compared to conventional chemical and antibody drugs.

Supplementary Information

The online version contains supplementary material available at <https://doi.org/10.1186/s12951-024-02943-1>.

Supplementary Material 1

Author contributions

Miaomiao Zhang and Xinyue Lu contributed equally to this work. Experimental design involved Miaomiao Zhang, Xinyue Lu, Jingbo Zhang, Ge Li and Fengying Sun. Data collection and analysis were conducted by Miaomiao Zhang, Xinyue Lu, Li Zhao and Jingqiu Dou. Manuscript drafting were performed by Miaomiao Zhang and Xinyue Lu. Project management was overseen by Fengying Sun. Lastly, review and revisions were carried out by Miaomiao Zhang, Xinyue Lu, Fengying Sun and Lifu Luo.

Funding

This work was supported by the International Cooperation Project (No.20220402036GH, No.20210402045GH) of Jilin Province Science and Technology Development Plan Project.

Data availability

No datasets were generated or analysed during the current study.

Declarations

Ethics approval and consent to participate

All the experimental procedures that had been conducted adhered to ethical guidelines and were approved by the Laboratory Animal Ethics and Welfare Committee of Jilin University (Approval No. SY202306034).

Consent for publication

All authors read and approved the final manuscript.

Competing interests

The authors declare no competing interests.

Author details

¹Key Laboratory for Molecular Enzymology and Engineering of Ministry of Education, School of Life Sciences, Jilin University, Changchun 130012, China

²Department of Ophthalmology, The Second Hospital of Jilin University, Jilin University, Changchun 130041, China

Received: 18 April 2024 / Accepted: 20 October 2024

Published online: 13 November 2024

References

1. Ambati J, Fowler BJ. Mechanisms of age-related macular degeneration. *Neuron*. 2012;75:26–39.
2. Campagne ML, LeCouter J, Yaspan BL, Ye WL. Mechanisms of age-related macular degeneration and therapeutic opportunities. *J Pathol*. 2014;232:151–64.
3. Guymier RH, Campbell TG. Age-related macular degeneration. *Lancet*. 2023;401:1459–72.
4. Rosenfeld PJ, Brown DM, Heier JS, Boyer DS, Kaiser PK, Chung CY, Kim RY. Ranibizumab for neovascular age-related macular degeneration. *N Engl J Med*. 2006;355:1419–31.
5. Papadopoulos N, Martin J, Ruan Q, Rafique A, Rosconi MP, Shi EG, Pyles EA, Yancopoulos GD, Stahl N, Wiegand SJ. Binding and neutralization of vascular endothelial growth factor (VEGF) and related ligands by VEGF trap, ranibizumab and bevacizumab. *Angiogenesis*. 2012;15:171–85.
6. Solomon SD, Lindsley K, Vedula SS, Krzystolik MG, Hawkins BS. Anti-vascular endothelial growth factor for neovascular age-related macular degeneration. *Cochrane Database Syst Rev*. 2019;8:CD005139.
7. Tranos P, Vacalis A, Asteriadis S, Koukoulas S, Vachtsevanos A, Perganta G, Georgalas I. Resistance to anti-vascular endothelial growth factor treatment in age-related macular degeneration. *Drug Des Devel Ther*. 2013;7:485–90.
8. Falavarjani KG, Nguyen QD. Adverse events and complications associated with intravitreal injection of anti-VEGF agents: a review of literature. *Eye*. 2013;27:787–94.
9. Palmieri EM, Menga A, Martin-Perez R, Quinto A, Riera-Domingo C, De Tullio G, Hooper DC, Lamers WH, Ghesquiere B, McVicar DW, et al. Pharmacologic or genetic targeting of glutamine synthetase skews macrophages toward an M1-like phenotype and inhibits tumor metastasis. *Cell Rep*. 2017;20:1654–66.
10. Eelen G, Dubois C, Cantelmo AR, Cantelmo AR, Goveia J, Bruning U, DeRan M, Jarugumilli G, van Rijssel J, Saladino G, et al. Role of glutamine synthetase in angiogenesis beyond glutamine synthesis. *Nature*. 2018;561:63–9.
11. Huang H, Vandekerke S, Kalucka J, Bierhansl L, Zecchin A, Bruning U, Visnagri A, Yuldasheva N, Goveia J, Cruys B, et al. Role of glutamine and interlinked asparagine metabolism in vessel formation. *EMBO J*. 2017;36:2334–52.
12. Li X, Sun X, Carmeliet P. Hallmarks of endothelial cell metabolism in health and disease. *Cell Metab*. 2019;30:414–33.
13. Mazzone M, Bergers G. Regulation of blood and lymphatic vessels by immune cells in tumors and metastasis. *Annu Rev Physiol*. 2019;81:535–60.
14. Draoui N, de Zeeuw P, Carmeliet P. Angiogenesis revisited from a metabolic perspective: role and therapeutic implications of endothelial cell metabolism. *Open Biol*. 2017;7:170219.
15. Huang XG, Zhou GH, Wu WY, Duan YJ, Ma GE, Song JY, Xiao R, Vandenberghe L, Zhang F, D'Amore PA, et al. Genome editing abrogates angiogenesis *in vivo*. *Nat Commun*. 2017;8:112.
16. Pickar-Oliver A, Gersbach CA. The next generation of CRISPR-Cas technologies and applications. *Nat Rev Mol Cell Biol*. 2019;20:490–507.

17. Hsu PD, Lander ES, Zhang F. Development and applications of CRISPR-Cas9 for genome engineering. *Cell*. 2014;157:1262–78.
18. Stadtmayer EA, Fraietta JA, Davis MM, Cohen AD, Weber KL, Lancaster E, Mangan PA, Kulikovskaya I, Gupta M, Chen F, et al. CRISPR-engineered T cells in patients with refractory cancer. *Science*. 2020;367:1001.
19. Eyquem J, Mansilla-Soto J, Giavridis T, van der Stegen SJC, Hamieh M, Cunanan KM, Odak A, Goenen M, Sadelain M. Targeting a CAR to the TRAC locus with CRISPR/Cas9 enhances tumour rejection. *Nature*. 2017;543:113–7.
20. Haapaniemi E, Botla S, Persson J, Schmieler B, Taipale J. CRISPR-Cas9 genome editing induces a p53-mediated DNA damage response. *Nat Med*. 2018;24:927–30.
21. Lino CA, Harper JC, Carney JP, Timlin JA. Delivering CRISPR: a review of the challenges and approaches. *Drug Deliv*. 2018;25:1234–57.
22. Nguyen DN, Roth TL, Li PJ, Chen PA, Apathy R, Mamedov MR, Vo LT, Tobin VR, Goodman D, Shifrut E, et al. Polymer-stabilized Cas9 nanoparticles and modified repair templates increase genome editing efficiency. *Nat Biotechnol*. 2020;38:44–9.
23. Batrakova EV, Kim MS. Using exosomes, naturally-equipped nanocarriers, for drug delivery. *J Control Release*. 2015;219:396–405.
24. Kim SM, Yang Y, Oh SJ, Hong Y, Seo M, Jang M. Cancer-derived exosomes as a delivery platform of CRISPR/Cas9 confer cancer cell tropism-dependent targeting. *J Control Release*. 2017;266:8–16.
25. Usman WM, Pham TC, Kwok YY, Vu LT, Ma V, Peng BY, San Chan Y, Wei LK, Chin SM, Azad A, et al. Efficient RNA drug delivery using red blood cell extracellular vesicles. *Nat Commun*. 2018;9:23359.
26. Li ZL, Zhou XY, Wei MY, Gao XT, Zhao LB, Shi RJ, Sun WQ, Duan YY, Yang GD, Yuan LJ. In vitro and in vivo RNA inhibition by CD9-HuR functionalized exosomes encapsulated with miRNA or CRISPR/dCas9. *Nano Lett*. 2019;19:19–28.
27. Yan Y, Du CC, Duan XX, Yao XH, Wan JJ, Jiang ZM, Qin ZY, Li WQ, Pan LZ, Gu ZY, et al. Inhibiting collagen I production and tumor cell colonization in the lung via miR-29a-3p loading of exosome-/liposome-based nanovesicles. *Acta Pharm Sin B*. 2022;12:939–51.
28. Lin Y, Wu JH, Gu WH, Huang YL, Tong ZC, Huang LJ, Tan JL. Exosome-liposome hybrid nanoparticles deliver CRISPR/Cas9 system in MSCs. *Adv Sci*. 2018;5:1700611.
29. Campochiaro PA. Ocular neovascularization. *J Mol Med*. 2013;91:311–21.
30. Liu J, Wei T, Zhao J, Huang YY, Deng H, Kumar A, Wang CX, Liang ZC, Ma XW, Liang XJ. Multifunctional aptamer-based nanoparticles for targeted drug delivery to circumvent cancer resistance. *Biomaterials*. 2016;91:44–56.
31. Huang Y, Liu X, Zhu J, Chen Z, Yu L, Huang X, Dong C, Li J, Zhou H, Yang Y, Tan W. Enzyme core spherical nucleic acid that enables enhanced cuproptosis and Antitumor Immune Response through alleviating Tumor Hypoxia. *J Am Chem Soc*. 2024;146:13805–16.
32. Liu XL, Li F, Dong ZL, Gu C, Mao DS, Chen JQ, Luo L, Huang YT, Xiao J, Li ZC, Liu Z, Yang Y. Metal-polyDNA nanoparticles reconstruct osteoporotic micro-environment for enhanced osteoporosis treatment. *Sci Adv*. 2023;9:eadf3329.
33. Liang C, Li FF, Wang LY, Zhang ZK, Wang C, He B, Li J, Chen ZH, Shaikh AB, Liu J, Wu XH, Peng SL, Dang L, Guo BS, He XJ, Au DWT, Lu C, Zhu HL, Zhang BT, Lu AP, Zhang G. Tumor cell-targeted delivery of CRISPR/Cas9 by aptamer-functionalized lipopolymer for therapeutic genome editing of *VEGFA* in osteosarcoma. *Biomaterials*. 2017;147:68–85.
34. Gao HL, Qian J, Cao SJ, Yang Z, Pang ZQ, Pan SQ, Fan L, Xi ZJ, Jiang XG, Zhang QZ. Precise glioma targeting of and penetration by aptamer and peptide dual-functioned nanoparticles. *Biomaterials*. 2012;33:5115–23.
35. Luo ZM, Yan ZQ, Jin K, Pang Q, Jiang T, Lu H, Liu XP, Pang ZQ, Yu L, Jiang XG. Precise glioblastoma targeting by AS1411 aptamer-functionalized poly (l-gamma-glutamylglutamine)-paclitaxel nanoconjugates. *J Colloid Interface Sci*. 2017;490:783–96.
36. Vivanco-Rojas O, Garcia-Bermudez MY, Iturriga-Goyon E, Rebollo W, Buentello-Volante B, Magana-Guerrero FS, Bates P, Perez-Torres A, Garfias Y. Corneal neovascularization is inhibited with nucleolin-binding aptamer, AS1411. *Exp Eye Res*. 2020;193:107977.
37. Guo JW, Gao XL, Su LN, Xia HM, Gu GZ, Pang ZQ, Jiang XG, Yao L, Chen J, Chen HZ. Aptamer-functionalized PEG-PLGA nanoparticles for enhanced anti-glioma drug delivery. *Biomaterials*. 2011;32:8010–20.
38. Mao DS, Dong ZL, Liu XL, Li WX, Li HY, Gu C, Chen GH, Zhu XL, Yang Y. An Intelligent DNA nanoreactor for easy-to-read in Vivo Tumor Imaging and Precise Therapy. *Angew Chem Int Ed Engl*. 2024;63:e202311309.
39. Ireson CR, Kelland LR. Discovery and development of anticancer aptamers. *Mol Cancer Ther*. 2006;5:2957–62.
40. Abcouwer SF, Lukasczewicz GC, Ryan US, Souba WW. Molecular regulation of lung endothelial glutamine synthetase expression. *Surgery*. 1995;118:325–34.
41. Zhang JX, Zhu JY, Zhao LZ, Mao K, Gu Q, Li DL, Zhao JH, Wu XW. RGD-modified multifunctional nanoparticles encapsulating salvianolic acid A for targeted treatment of choroidal neovascularization. *J Nanobiotechnol*. 2021;19:196.
42. Liang Y, Kong LJ, Zhang YL, Zhang YH, Shi MS, Huang JQ, Kong HY, Qi SY, Yang YL, Hong JX. Transfer RNA derived fragment, tRF-Glu-CTC, aggravates the development of neovascular age-related macular degeneration. *Theranostics*. 2024;14:1500–16.
43. Mettu PS, Allingham MJ, Cousins SW. Incomplete response to Anti-VEGF therapy in neovascular AMD: exploring disease mechanisms and therapeutic opportunities. *Prog Retin Eye Res*. 2021;82:100906.
44. Zhang CH, Tang SS, Wang ML, Li LH, Li J, Wang DK, Mi X, Zhang YY, Tan XY, Yue SJ. Triple-punch strategy exosome-mimetic nanovesicles for Triple negative breast Cancer Therapy. *ACS Nano*. 2024;18:5470–82.
45. Wan T, Zhong JF, Pan Q, Zhou TH, Ping Y, Liu XR. Exosome-mediated delivery of Cas9 ribonucleoprotein complexes for tissue-specific gene therapy of liver diseases. *Sci Adv*. 2022;8:9435.
46. Yao XG, Lyu P, Yoo K, Yadav MK, Singh R, Atala A, Lu BS. Engineered extracellular vesicles as versatile ribonucleoprotein delivery vehicles for efficient and safe CRISPR genome editing. *J Extracell*. 2021;10:e12076.
47. Duan L, Xu LM, Xu X, Qin ZA, Zhou XY, Xiao Y, Liang YJ, Xia J. Exosome-mediated delivery of gene vectors for gene therapy. *Nanoscale*. 2021;13:1387–97.
48. Sabanayagam C, Banu R, Chee ML, Lee R, Wang YX, Tan G, Jonas JB, Lamoureux EL, Cheng CY, Klein BEK. Incidence and progression of diabetic retinopathy: a systematic review. *Lancet Diabetes Endo*. 2019;7:140–9.
49. Hellstrom A, Smith LEH, Dammann Olaf. Retinopathy of prematurity. *Lancet*. 2013;382:1445–57.

Publisher's note

Springer Nature remains neutral with regard to jurisdictional claims in published maps and institutional affiliations.